Problem 20.3. Show that for $h\nu_1 \gg kT_{\text{eff}}$, the average ionizing photon energy $h\bar{\nu} \approx kT_{\text{eff}}$, where the luminosity at r is Planckian. Note that

$$\int_x^\infty e^{-t}\frac{dt}{t} \simeq \frac{e^{-x}}{x}\left(1 - \frac{1}{x} + \frac{2!}{x^2} + \cdots\right) \qquad x \gg 1.$$

Problem 20.4. Set an upper limit to the number of photoionizations from photons produced by recombination of He^+ to excited states of He^0. The recombination coefficients $\alpha'(H^0) \approx \alpha'(He^0)$ to about 5 percent.

The principal heating mechanism for gaseous nebulae is of the form (20.9), and should in principle include a contribution for $\gamma + He^0 \rightarrow He^+ + e^-$. In the hottest planetary nebulae, an additional contribution may be needed to describe the photoionization $\gamma + He^+ \rightarrow He^{+2} + e^-$.

20.3. Energy Loss Mechanisms

Effective cooling of gaseous nebulae depends on the production of photons whose energy is too low to lead to further ionization of H or He. Once produced, these photons will leave the nebula. Three primary mechanisms can be identified: recombination of H^+ and He^+; collisional excitation by electrons of the atoms or ions having excited states lying only a few eV or less above their ground states; and free-free transitions (*Bremsstrahlung*) of electrons in the field of positive ions. Each process can be expressed as an energy-loss rate per unit volume, which counteracts the photoionization heating rate discussed in Section 20.2.

Radiative Recombination

The radiative-recombination loss rate can be obtained directly from the discussion of (20.5). Each recombination removes from the gas an energy equal to that of the captured electron $\epsilon_e = m_e v^2/2$. The energy-loss rate Λ_R is obtained if the electron flux in (20.5) is replaced by the electron energy flux $\epsilon_e n_e v f(v)$, and the result multiplied by the density of target particles $n(H^+)$:

$$\Lambda_R = n(H^+)\sum_{n=2}^{\infty}\int_0^\infty n_e v\,\frac{1}{2}m_e v^2\sigma_n(v)f(v)\,dv$$
$$= n(H^+)n_e\beta'(H^0)kT_e. \qquad (20.11)$$

The second line defines β'; recombination to the ground state $n = 1$ has been excluded, since the emitted photon will reionize another H^0 rather than escape from the nebula. Recombination is assumed to occur from the thermalized electron distribution characterized by the kinetic temperature T_e, as outlined in the discussion preceeding (20.5). Because $\sigma_n(v) \approx v^{-2}$, low-energy electrons are preferentially captured, and their average energy is slightly below the average of the initial distribution. Consequently, if the equilibrium state of the gas were defined by $\Gamma = \Lambda_R$, then its temperature T_e would exceed T_{eff}. An expression similar to (20.11) could also be written for the energy loss due to recombination of He^+, or other ions present. The contribution of these processes is small, since they are proportional to the ion density. In fact, generalizing (20.11) to other ions, we find that the net recombination cooling rate is

$$\Lambda_R = \Lambda_R(H^+) + \Sigma\Lambda_R(X_k^i)$$
$$= \Lambda_R(H^+)\left[1 + \sum\frac{n(X_x^i)}{n(H^+)}\frac{\beta'(X_k^i)}{\beta'(H^0)}\right], \qquad (20.12)$$

where the sum covers all atomic species k and all ionization states i of the gas. Evidently the contribution of He^+ is small (less than 10 percent), and that of the heavier elements is, in total, less than about 1 percent. In practice He^+ recombination is included when calculating Λ_R, but the recombination of heavier elements (such as O^+, O^{+2}, and N^+) is omitted.

Collisional Excitation

The most effective cooling mechanism in gaseous nebulae is the emission of forbidden-transition radiation by intermediate-mass ions that have been excited by collisions with electrons to states whose energies are roughly kT_e above the ground state. Figure 20.3 shows the low-lying energy levels of three of the most important coolants in gaseous nebulae, and the principal transitions in the visible spectrum. The lowest-energy transitions in O^+ produce lines in the violet. Transitions in O^{+2} produce lines in the green, and the transitions in N^+ lie in the red. Spontaneous emission rates A_{mn} vary from about one per sec to 4×10^{-5} sec^{-1} for these forbidden processes. Although the abundances of intermediate-mass ions are extremely low (see Figure 18.2), the radiation they emit cannot excite or ionize other elements and therefore escapes from the nebula.

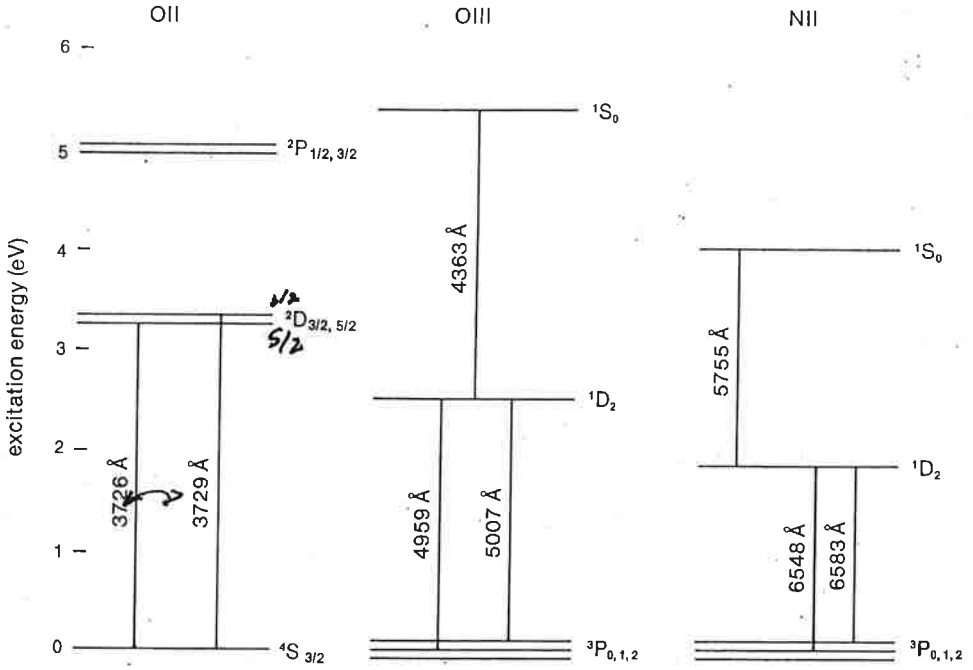

Figure 20.3. Low-lying energy levels of OII, OIII, and NII, the primary coolant ions in interstellar HI regions. Excitation energy relative to the ground state of the ion is shown in eV at left. Wavelength of transitions in Å is given next to each transition.

Electron-ion collisions populate excited states in the ions, whereas radiative (spontaneous) emissions to the ground state depopulate them. Collisions can also depopulate excited states, in which case the excitation energy goes into kinetic energy of the electron rather than into radiation. Consider a typical electron-ion collision that excites an ion from state i to j (i is usually the ground state in a nebula). The excitation cross section for this process is given by

$$\sigma_{ij} = \frac{\pi\hbar^2}{m_e^2 v^2}\frac{\Omega_{ij}}{g_i} = \frac{4.21}{v^2}\frac{\Omega_{ij}}{g_i}\ \text{cm}^2, \qquad (20.13)$$

where v is the electron velocity, and g_i the statistical weight of the initial state of the ion; Ω_{ij}, which depends weakly on velocity, is called the *collision strength*. It is dimensionless, and is usually of order unity under nebular conditions. For $T_e \approx 7{,}000$ K, $v \approx 6 \times 10^7$ cm/sec and $\sigma_{ij} \approx 10^{-15}\,(\Omega_{ij}/g_i)$ cm^2. If $m_e v^2/2 < h\nu_{ij}$, the excitation energy, then the cross section is zero.

Problem 20.5. Use the principle of detailed balance to show that the de-excitation cross section (used to calculate the rate of collision-induced transition from level j to level i) is

$$\sigma_{ji} = (g_i/g_j)\,(v_i/v_j)^2\,\sigma_{ij}. \qquad (20.14)$$

The rate of collisional de-excitation from level j to level i caused by electrons of velocity v is described by the product of the electron flux, the number density of target ions in the j^{th} excited state $n(X_k^j)$, and the de-excitation cross section; integrating the result over electron velocities, we find the rate per unit volume to be

$$n_e n(X_k^j)\, r_{ij} = n(X_k^j) \int_0^\infty n_e v \sigma_{ji}(v) f(v)\, dv. \qquad (20.15)$$

The electron-velocity distribution $f(v)$ is Maxwellian. Assuming that Ω_{ij} is a constant, we find that the

de-excitation rate becomes

$$n_e n(X_k^j) r_{ij} = n_e n(X_k^j) \left(\frac{2\pi}{kT_e}\right)^{1/2} \frac{\hbar^2}{m_e^{3/2}} \frac{\Omega_{ji}}{g_j} \qquad (20.16)$$

$$= 8.6 \times 10^{-6} \frac{n_e n(X_k^j)}{g_j T_e^{1/2}} \Omega_{ij} \text{ cm}^{-3} \text{ sec}^{-1}.$$

For typical nebular temperatures and abundances, the rate r_{ji} for the important coolants is roughly 10^{-7} cm^3/sec.

Problem 20.6. Show that the collisional excitation rate is given by

$$r_{ij} = (g_j/g_i) r_{ji} e^{-\chi_{ji}/kT_e}, \qquad (20.17)$$

where

$$\chi_{ji} = m_e(v_j^2 - v_i^2)/2,$$

v_j is the velocity of the electron exciting the ion, and v_i is the velocity inducing de-excitation. Recall that no photon is emitted in collisional de-excitation.

Expressions (20.16) and (20.17) for r_{ij} and r_{ji} may be used to obtain the collisional cooling rate. For most nebular coolants (such as those in Figure 20.3), the initial or final levels are multiple, and transitions among all states must be considered. For example consider a simple two-level ion (such as the transition between the $^1S_0$ and $^1D_2$ states of O^{+2} or N^+ in Figure 20.3). The energy loss per unit volume per second due to the spontaneous emission of a photon from a collisionally excited state 2 to the lower level 1 is

$$\Lambda_0 = n(X_k^2) A_{21} h\nu_{21}, \qquad (20.18)$$

where $n(X_k^2)$ is the number density of coolant ions in the excited state. In statistical equilibrium the number of upward transitions (due to collisions) equals the number of downward transitions (due to collisions and spontaneous decay):

$$n(X_k^2)(n_e r_{21} + A_{21}) = n_e n(X_k^1) r_{12}. \qquad (20.19)$$

The rates r_{21} and r_{12} are given by (20.16) and (20.17). Solving (20.19) for the ratio of ions in the excited and ground states, and substituting into (20.18) yields

$$\Lambda_{c,21} = \frac{n_e n(X_k^1) r_{12} h\nu_{21}}{1 + n_e r_{21}/A_{21}} \text{ erg cm}^{-3} \text{ sec}^{-1}. \qquad (20.20)$$

In nebulae the electron density n_e is usually low enough that spontaneous emission dominates collisional de-excitations. Taking the $n_e \to 0$ limit of $\Lambda_{c,21}$, we find

$$\Lambda_{c,21} \simeq n_e n(X_k^1) h\nu_{21} r_{12} \qquad (20.21)$$

$$= n_e n(X_k^1) h\nu_{21} \frac{g_2}{g_1} e^{-\chi/kT_e} r_{21}$$

$$= n_e n(X_k^1) h\nu_{21} \frac{e^{-\chi/kT_e}}{g_1} \frac{8.6 \times 10^{-6}}{T_e^{1/2}} \Omega(1, 2),$$

using (20.16), and $\chi = h\nu_{21}$. At temperatures well below χ/k, the exponential in Λ_c dominates, and the cooling rate is low; but at T_e of order $0.2\chi/k$, it increases rapidly, reaching a maximum at $T_e \approx 2\chi/k$. Thereafter Λ_c decreases approximately as $T^{-1/2}$ for fixed $n(X_k^i)$. For the primary coolants (O^+, O^{+2}, and N^+) at $T_e \approx 7{,}000$ K, the ratio $\Lambda_c/n_e n(H^0)$ is of order 10^{-24} erg cm^3/sec.

Problem 20.7. What is Λ_c in the limit $n_e \to \infty$? Explain why the form of this result corresponds to thermal equilibrium.

When forbidden transitions involve more than one level (g_i or $g_j > 1$), Λ_c may be constructed as follows. First, the net cooling rate for the ion k due to transitions from the multiple levels j to the state i is

$$\Lambda_{c,k} = \sum_i n(X_k^i) \sum_{j>i} A_{ji} h\nu_{ji}. \qquad (20.22)$$

The relation between the population of various levels j and i is given by the obvious extension of (20.19), resulting in one equation for each possible transition (collisional or spontaneous). Finally, for each pair of levels between which transitions can occur, the rates $r_{ij}^{(k)}$ analogous to (20.16) may be obtained. Finally, the total number of ions in the ground or excited states

must equal the number of ions in the gas. This set of equations can be used to construct the net cooling rate (20.22) as a function of n_e, $n(X_k^1)$, and the electron temperature. Once the fractional abundance of the ionized elements has been decided (see Section 20.5), the cooling rate Λ_c becomes a function of T_e.

Bremsstrahlung

A continuous spectrum is emitted by thermal electrons that scatter off ions in the gas. Most of the energy is emitted in the radio and in the infrared, and can readily escape the nebula. The loss rate for ions of number density n_i is

$$\Lambda_{ff} \simeq \frac{2^5 e^6 \pi Z^2}{3^{3/2} h m_e c^3} \left(\frac{2\pi k T_e}{m_e}\right)^{1/2} n_e n_i$$
$$= 1.4 \times 10^{-27} Z^2 T_e^{1/2} n_e n_i \text{ erg cm}^{-3} \text{ sec}^{-1}. \quad (20.23)$$

Usually energy loss via Λ_{ff} is small compared with that from recombination and collisional processes, unless the ion density is extremely small. Note that (20.23) would produce losses from protons in a pure hydrogen nebula in which Λ_c would be zero.

The net cooling rate for a gaseous nebula is the sum of radiative recombination losses (20.12), collisional losses (20.22) for all coolant ions, and *Bremsstrahlung* (20.23).

20.4. Structure Equations

In principle the structure of an HII region or a planetary nebula could be obtained from the spectrum L_ν of the ionizing star, as well as the density distribution and abundances of elements in the surrounding medium. From these could be obtained the ionization states $X_k^i(\mathbf{r})$ and the plasma temperature $T_e(\mathbf{r})$ at each point in the nebula. These would be used to construct the spectrum of emitted radiation, including lines and continuum from the radiative transfer equation. Unfortunately, many processes produce lines in the ultraviolet or infrared that are not easily observed through the atmosphere. Furthermore, it is difficult to resolve the internal structure in nebulae with enough accuracy to pinpoint the spatial origin of individual spectral components. Because of these limitations, most models of nebulae assume spherical symmetry.

All the processes to be considered in this section operate on time-scales that are short relative to the time required for large-scale changes in the structure of nebulae. The structure equations are limited to a description of the steady state.

The input for model nebulae consists of those quantities specifying the energy input of the ionizing star: $L_\nu(R)$ in ergs cm^{-2} sec^{-1} Hz^{-1} ster^{-1}; the stellar radius R and inner radius of the nebula r_0; as well as the density distribution $\rho(\mathbf{r})$ and relative abundances $n(X_k)/n(\mathrm{H})$ of all elements X_k. The radiation intensity I_ν at point r in the nebula consists of two parts:

$$I_\nu = I_\nu^s + I_\nu^d; \quad (20.24)$$

the first is the stellar component, and the second is due to emission from atoms in the nebula itself. Defining the mean intensity as (5.2), we find the stellar component to be

$$4\pi J_\nu^s = L_\nu(r)/4\pi r^2. \quad (20.25)$$

The transport equations may be written in terms of each component. For the stellar component,

$$\frac{dL_\nu(r)}{dr} = -k_\nu L_\nu(r), \quad (20.26)$$

$$\frac{dI_\nu^s}{ds} = -k_\nu I_\nu^d + j_\nu. \quad (20.27)$$

The emission coefficient j_ν describes the photons emitted from the gas, and does not include direct radiation from the ionizing star. The absorption coefficient will be defined as

$$k_\nu = \sum_i n_i a_\nu(i)$$
$$\simeq n(\mathrm{H}^0) a_\nu(\mathrm{H}^0) + n(\mathrm{He}^0) a_\nu(\mathrm{He}^0). \quad (20.28)$$

In general the sum is over all ions or atoms that can be further ionized by the radiation source (20.25).

Equations describing the ionization state of the gas as a function of the ionizing star's luminosity are of the form (20.7) for H and He, but require modification for the intermediate-mass ions. For these, the source $J_\nu(r)$

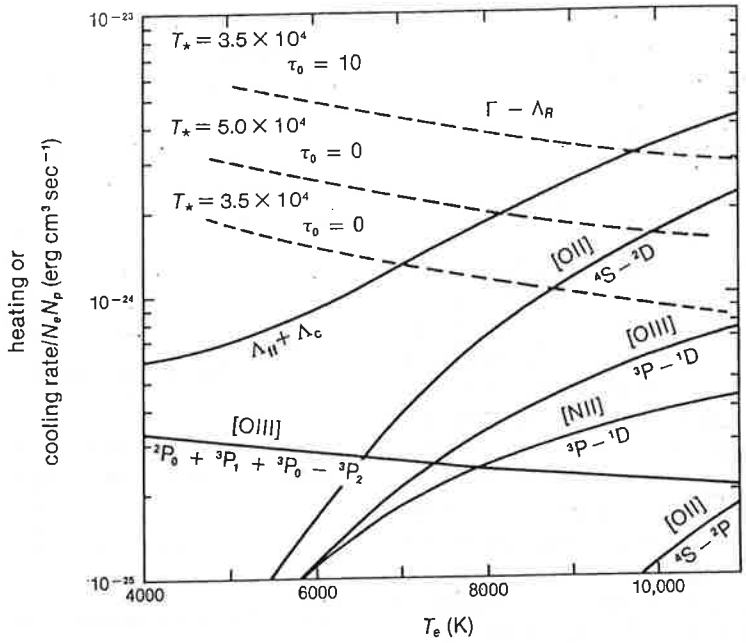

Figure 20.4. Heating and cooling rates versus temperature. Dashed curves give $\Gamma - \Lambda_R$ for three stellar input spectra (T_* denotes the spectral temperature), and τ_o is the optical depth of the medium at the ionization limit. The radiative cooling curve is labeled $\Lambda_{II} + \Lambda_c$. dominant contributions to the radiative cooling are shown by the light solid curves.

includes the diffuse emission from the gas as well as the stellar emission (as we will see). Thus for each ionic state in the gas, an equation of the general form (20.7) results. Together these equations describe the relative concentrations of ions in the nebula.

Finally, the thermal state of gas is described by the energy equilibrium equation

$$\Lambda_c + \Lambda_{II} + \Lambda_R = \Gamma, \qquad (20.29)$$

which states that the net energy loss equals the energy gain per unit volume per second. The quantities in (19.29), which are defined in Sections 20.2 and 20.3, are functions of the density (assumed given), the ionic concentrations (derived from ionization equilibrium), and T. Therefore (20.29) describes T_e as a function of these variables and $L_\nu(r)$. The heating function Γ does not depend on T_e, but the cooling rates Λ_R (20.11), Λ_c (20.21), and Λ_{II} (20.23) do contain T_e. In practice the procedure outlined in the preceding must be solved iteratively, until the value of T_e used to evaluate the ionization state and the terms in (20.29) and the derived T_e converge.

Several general conclusions about the equilibrium state of a nebula follow from (20.29) and the expressions for Γ and the loss rates developed in earlier sections. First, because each term in (20.29) varies linearly with n_e (in the low-density limit), the equilibrium temperature T_e is independent of n_e. Each term is also proportional to the density of an ion in the gas. Therefore, the equilibrium state is independent of the density, though it does depend through Λ_c on the abundances of coolant ions relative to $n(H^+)$. Finally, at high densities, Λ_c is independent of n_e; therefore, as n_e increases, so must T_e.

Problem 20.8. Show that the preceding conclusions follow for the simple case of a nebula containing only hydrogen and a single coolant ion.

Figure 20.4 shows the heating and cooling rates as a function of T_e for a simple model of an HII region in

which the elements have abundances comparable to those shown by the open circles in Figure 18.1. Here 80 percent of the coolant ions are assumed to be singly ionized, and the rest doubly ionized, and

$$n(H^+)/n(H^+ + H^0) = 0.9.$$

The dashed curves represent three possible results for the net photoionization heating $\Gamma - \Lambda_R$. The lower two curves result for stellar effective temperatures T_{eff} of 35,000 K (spectral type O7) and 50,000 K (spectral type O5) at points near the star. The upper dashed curve is at an optical depth = 10; the net heating is greater there because the average photon energy $h\bar{\nu}$ (20.10) increases with distance. The thin solid lines labeled by an ionic state and the electronic transition in the ion (see Figure 20.3) are the contributions to Λ_c. At low electron temperatures, transitions between the triplet P states in O^{+2} are the dominant cooling mechanism, but at higher values O^+ becomes the more important. Notice the rapid rise in the contributions of O^+, N^+, and O^{+2} that results when T_e almost doubles. The heavy solid curve gives the net cooling rate $\Lambda_{ff} + \Lambda_c$ including all ions, and its intersection with the dashed curve defines the electron temperature of the nebulae. Depending on the distance from the ionizing star (optical depth) and assumed surface brightness, T_e varies from 7,000 K to 9,000 K. The density n_e is low enough in this example for collisional de-excitation to be negligible. If n_e approaches 10^4 cm^{-3}, collisional de-excitation becomes important, and the relative importances of various ionic cooling terms change. However, the equilibrium T_e increases by only about 20 percent.

Problem 20.9. Fluctuations in T_e can occur at arbitrary points in a nebula. Show that the equilibrium state defined by (19.29) and shown in Figure 20.4 is stable against small variations in T_e.

20.5. Model Nebulae

The results developed in Section 20.4 can be applied to a model of a planetary nebula composed of H, He, and trace ions. The initial data required to solve the structure equations, discussed at the beginning of Section 20.4, will be summarized here for convenience. They are:

$$\begin{pmatrix}\text{stellar luminosity}\\ \text{at stellar surface } R\end{pmatrix} = L_\nu(R) \text{ erg Hz}^{-1}\text{sec}^{-1}; \quad (20.30)$$

$$\text{inner radius of nebula} = r_0 \quad (20.31)$$

$$n(\text{He})/n(\text{H}) \quad (20.32)$$

$$n(X_k)/n(\text{H}) \quad (20.33)$$

$$\rho(r) = m_H[n(\text{H}) + 4n(\text{He})]. \quad (20.34)$$

The number density of a specific ionic state (i) of an element X_k will be denoted by $n(X_k^i)$. Thus in (20.32)

$$n(\text{H}) = n(\text{H}^+) + n(\text{H}^0),$$

where H^0 denotes neutral hydrogen. First, the stellar energy input can be obtained at $r > R$ from (20.26):

$$L_\nu(r) = L_\nu(R)e^{-\tau_\nu(r)}, \quad (20.35)$$

where

$$\tau_\nu(r) = \int_{r_0}^{r} k_\nu(r')dr' \quad (20.36)$$

and the absorption coefficient is given by the second line of (20.28). In general r_0 will not equal R, but $L_\nu(r_0) = L_\nu(R)$. Evidently, $\tau_\nu(r)$ is the optical depth of the stellar radiation measured into the nebula, and $L_\nu(r)$ gives the stellar energy spectrum (including effects of absorption) carried across a sphere of radius r in the nebula. Although (20.35) is a formal solution for $L_\nu(r)$, it can not be evaluated until the abundances of absorbing atoms (H^0 and He^0) are specified.

Ionization State (H *and* He)

We will assume at the outset that the nebula contains no He^{+2}, that $n(\text{He})/n(\text{H}) \approx 0.1$, and that the total abundance of intermediate-mass ions

$$\sum_k n(X_k)/n(\text{H}) = 10^{-3}.$$

The first step in constructing a model nebula is to find a value for the ionization state of H and He, assuming a local value for T_e; the latter must be checked against the value derived from the energy-balance equation (20.29) for consistency. It is difficult to solve the structure equations in terms of the total intensity (stellar plus diffuse components). In most cases one of two approximations may be made.

In the first, the diffuse radiation (that emitted by atoms in the gas) escapes directly from the nebula upon emission, and all ionization is due to the stellar component. With these assumptions, the absorption term in the transfer equation (20.27) is absent, and

$$I_\nu^d = \int j_\nu \, ds. \tag{20.37}$$

We call this the *thin limit;* it is applicable to low-density or small nebulae, and to the radiation emitted by coolant ions.

The second approximation is that the nebula is optically thick. Diffuse radiation is absorbed where it is created (*on-the-spot* approximation); the change in I_ν^d with path length is then small, and (20.27) becomes

$$I_\nu^d = j_\nu / k_\nu. \tag{20.38}$$

This limit applies to the photoionization processes that determine the ionization state of H and He, which we now consider.

Hydrogen recombination to all states except the ground state produces photons that can not ionize H^0 or He^0. We therefore write (20.7), excluding recombination to the ground state, and replacing $J_\nu(r)$ by $L_\nu(r)$, using (20.4), in the form

$$n(H^0) \int_{\nu_1}^{\infty} \frac{L_\nu(r)}{h\nu} \alpha_\nu(H^0) \, d\nu = 4\pi r^2 n_e n(H^+) \alpha'(H^0), \tag{20.39}$$

where $\nu_1 = 13.6$ eV. Recombination of He^+ to excited states of He^0 is more difficult; it can not ionize He^0, but can ionize H^0. It is customary to assume that all photons produced by He^+ recombination ionize H^0 but not He^0 (see Problem 20.4); the ionization state of He is then described, in analogy with (20.39) by

$$n(He^0) \int_{\nu_2}^{\infty} \frac{L_\nu(r)}{h\nu} a_\nu(He^0) \, d\nu = 4\pi r^2 n_e n(He^+) \alpha'(He^0) \tag{20.40}$$

with $\nu_2 = 24.5$ eV. Charge neutrality requires that the local abundances of He^+ and H^+ satisfy

$$n_e = n(H^+) + n(He^+). \tag{20.41}$$

The ionization state of the nebula is now specified; the stellar energy input given by (20.35), (20.36), and (20.28), together with the ionization equation (20.39) and (20.40), mass density (20.34), and charge neutrality (20.41), represent seven equations in eleven unknowns. Given the initial data $L_\nu(r)$, r_0, ρ, and $n(He)/n(H)$, they may be solved for $n(H^+)$, $n(H^0)$, $n(He^+)$, $n(He^0)$, and n_e. Figure 20.5 shows results for a model nebula as a function of distance from the ionizing star whose effective temperature $T = 3.5 \times 10^4$ K. In this model, $r_0 = 8 \times 10^{16}$ cm; the nebula consists of an inner sphere ($r \lesssim 1.75 \times 10^{17}$ cm) in which essentially all the H and He are singly ionized, surrounded by a shell 5.5×10^{16} cm thick containing He^0 and H^+. The transition between two ionization states is quite sharp. The outer boundary of the nebula, where $n(H^+)$ falls essentially to zero, is about 2.3×10^{17} cm from the ionizing star. Planetary nebulae are observed to range in diameter from 0.06 to 0.4 pc, and the effective temperature of the central star usually lies in the range 3 to 30×10^4 K.

The ionization structure established thus may then be used to obtain the intensity of the diffuse radiation emitted by the gas. Using the approximation (19.38) for an optically thick nebula, and remembering that j_ν and k_ν result almost entirely from H and He and are dependent only on the assumed T_e and on known ionization abundances, we can find I_ν^d. The stellar component (recall that the mean intensity is used) J_ν^s follows from the solution of (20.35) and (20.4).

Ionization State (Coolants)

The coolant ions occur with very low abundances relative to H or He, and essentially all their emitted radiation escapes from the nebula. This justifies treating them as if they were decoupled from the nebular gas (H and He) as a whole. Nevertheless, these trace elements play a dominant role in the energy budget of the nebula, and in setting the electron temperature. Given the results summarized in Figure 20.5, we can obtain the ionization state of the coolant ions as follows.

We assume first that all radiation from these ions escapes. Therefore, ionization is due to stellar photons

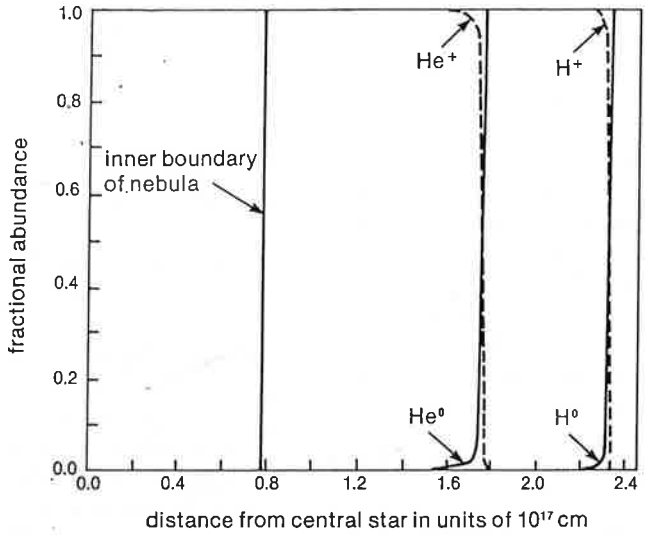

Figure 20.5. Fractional abundances of He^0 and H^0 (solid), and of He^+ and H^+ (dashed) in model nebula. (See Figures 20.6 and 20.7 also.)

and to photons in the diffuse component emitted by H and He. In statistical equilibrium the photoionization and recombination rates are equal, and an equation of the form

$$n(X_k^i) \int_{\nu_k}^{\infty} \frac{J_\nu}{h\nu} a_\nu(X_k^i)\, d\nu = n_e n(X_k^{i+1}) \alpha(X_k^{i+1}) \quad (20.42)$$

results for each ion k, and for each possible ionization state. Two comments about (20.42) are in order. First, the recombination coefficient includes recombination to the ground state, because the emitted photon is assumed to escape from the nebula. Second, the source J_ν is

$$4\pi J_\nu(r) = \int (I_\nu^d + I_\nu^s)\, d\Omega = J_\nu^s(r) + \int I_\nu^d\, d\Omega. \quad (20.43)$$

Finally, for each atomic species

$$n(X_k) = \sum_i n(X_k^i), \quad (20.44)$$

with the sum extending over all ionization states for which an equation of the form (20.42) is assumed. The set of equations (20.42) to (20.44) can be solved for the abundance $n(X_k^i)/n(\mathrm{H})$ for each ionic state, assuming that the total relative abundance $n(X_k)/n(\mathrm{H})$ is known. The final model may be used to predict the relative strength of emission lines as a function of the assumed abundances. In practice the latter are chosen so that the relative line strengths agree with these observations.

Figure 20.6 shows the most important ionic abundances $n(X_k^i)$ for the model. Oxygen, nitrogen, and neon occur in the singly and doubly ionized states within the nebula, but recombine to the neutral state across the outer boundary. Carbon, which is singly, doubly, and triply ionized within the nebula, exists as C^+ outside it. Notice that the transition between ionization states is gradual except near the outer boundary.

Thermal Equilibrium

The abundances shown in Figures 20.5 and 20.6 are now used to evaluate (20.29) for the kinetic temperature T_e of the electron gas. It will be recalled that T_e appears in the recombination coefficient (its dependence there is weak, $\approx T_e^{-1/2}$) and in the cooling rates Λ_c, and that one must assume an average value

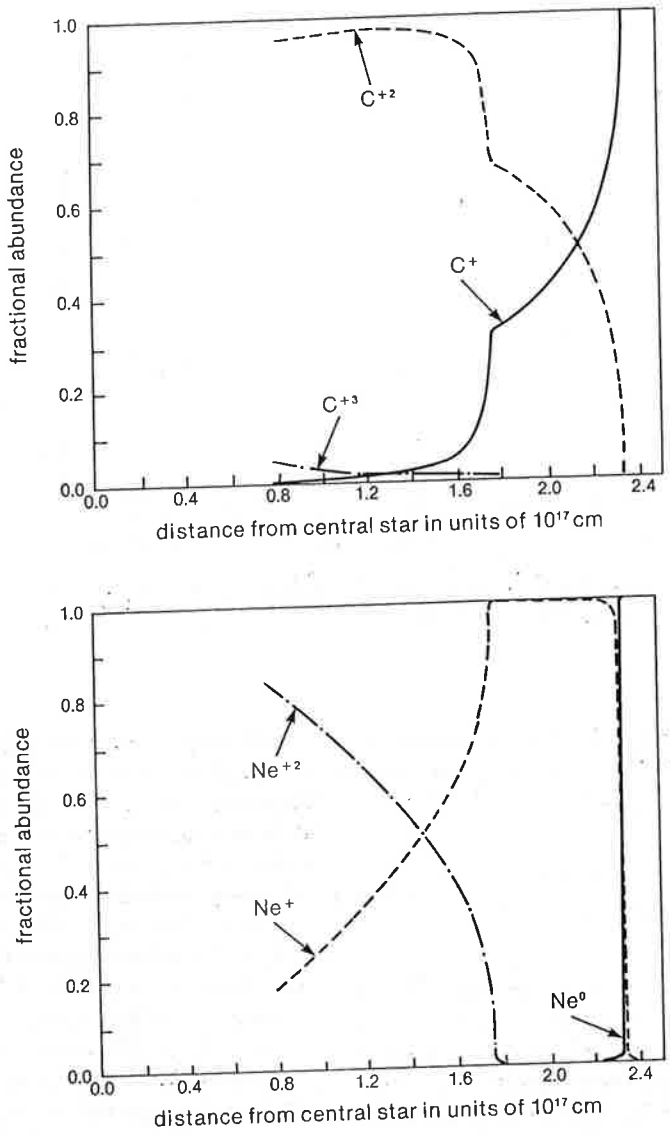

Figure 20.6. Fractional abundances of coolant ions in the model nebula shown in Figure 20.5.

initially in order to evaluate the ionic abundances and cooling rates. Therefore, if precise results are desired, the entire procedure may need to be repeated, using the T_e derived in the following as input for a new iteration of the structure equations. The following discussion applies in this case as well.

Let us assume initially that only H and the coolant ions are present in the nebula, so that the equation of thermal equilibrium becomes

$$h\bar{\nu} \equiv \frac{\beta'(\mathrm{H}^0) + \beta_{\mathrm{ff}}(\mathrm{H}^0)}{\alpha(\mathrm{H}^0)} kT_e + \frac{\Lambda_c}{n_e n(\mathrm{H}^+)\alpha(\mathrm{H}^0)} \tag{20.45}$$

with $h\bar{\nu}$ defined as in (20.10) and $\beta'(\mathrm{H}^0)$ as in (20.11). The *Bremsstrahlung* contribution $\beta_{\mathrm{ff}}(\mathrm{H}^0)$ follows immediately on comparison with (20.23); but this

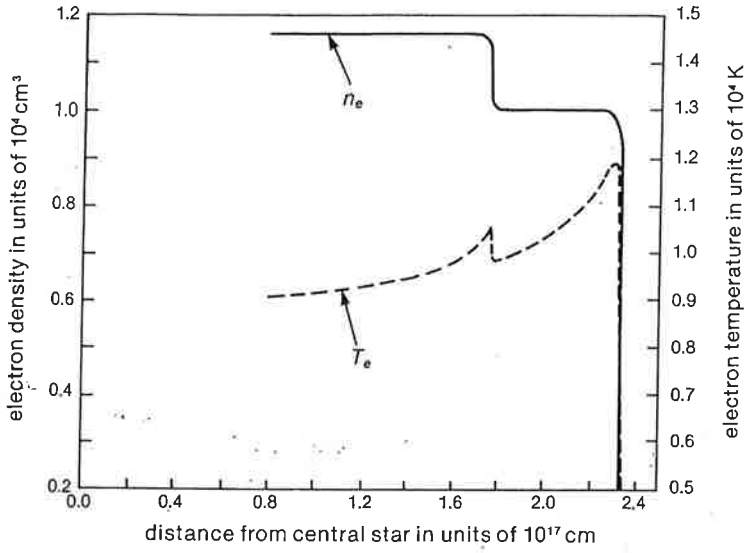

Figure 20.7. Temperature and electron number-density profiles in model nebula (see Figures 20.5 and 20.6).

effect is extremely small, and can be ignored here. Therefore, recalling (20.21) for the low-density regime ($n_e \ll 10^4$ cm^{-3}), we have

$$h\bar{\nu} \simeq \frac{\beta'(\mathrm{H}^0)}{\alpha(\mathrm{H}^0)} kT_e + \sum_{i,k} A_k \frac{n(X_k^i)}{n(\mathrm{A}^+)} \frac{e^{-\chi_i/kT_e}}{T_e^{1/2}}, \quad (20.46)$$

where A_k is a constant, and the summation in the last term is over all coolant ionic species present in the nebula. The energy-balance equation is transcendental in T_e, but may be solved numerically.

Several features of the solution can be seen in (20.46). First, we recall that the left-hand side $h\bar{\nu}$, which contains an integral over the photoionization cross section $a_\nu \sim (\nu_1/\nu)^3$, increases with distance into the nebula; see the discussion following (20.10). Consider the right-hand side of (20.46). For $T_e \lesssim$ several times χ_i, the collisional cooling terms increase or remain essentially constant with increasing T_e. Thus, since $h\bar{\nu}$ increases radially outward, so will T_e, until we reach the outer boundary of the nebula. At the boundary, $h\bar{\nu}$ continues to change slowly, but $n(\mathrm{H}^+)$ goes rapidly to zero (see Figure 20.5). The abundance of coolants changes across the outer boundary also, but the net effect is to replace one ionic coolant (O^+, for example) by another coolant (O^0). As a result, the collisional cooling terms in (20.46) dominate, and T_e must decrease abruptly. The equilibrium electron temperature therefore increases gradually with distance from the ionizing star, reaches its maximum value just behind the $\mathrm{H}^+ \rightarrow \mathrm{H}^0$ transition zone at the nebula's boundary, and then drops rapidly to values typical of the interstellar medium. Figure 20.7 shows T_e and n_e obtained numerically for the model (which includes heating from photoionization of He) corresponding to Figures 20.5 and 20.6. The reduction in n_e at $r \simeq 1.7 \times 10^{17}$ cm corresponds to He^+ recombination; since $n(\mathrm{He}) \simeq 0.1\, n(\mathrm{H})$, it is about a 10 percent effect, as expected. At the $\mathrm{He}^+ \rightarrow \mathrm{He}^0$ transition, the ratios $n(\mathrm{O}^+)/n(\mathrm{O})$ and $n(\mathrm{N}^+)/n(\mathrm{N})$ increase from relatively low values to essentially unity. Since these elements are extremely efficient coolants (Figure 20.4), the local electron temperature drops abruptly, as shown in Figure 20.7, but increases gradually until the outer boundary is reached.

In general, the value of T_e obtained from (20.45) will differ from the value assumed at the start of the calculation. If the difference is significant, then the entire process described above may be repeated using the new value of T_e as input for the next iteration. In practice the procedure usually converges rapidly. For planetary nebulae, such as the one described here, $T_e \approx 10^4$ K, though it rises to slightly higher values just

behind the $He^+ - He^0$ and $H^+ - H^0$ transition boundaries.

20.6. Relative Line Strengths

Much of the line emission observed in nebulae arises from the coolant ions, and their relative strength is one of the most useful probes of T_e, n_e, and the coolant abundances. Figure 20.3 shows the energy levels most frequently involved in line emission from nebulae; at $T_e \approx 10^4$ K, only the first two excited states are populated, and the ions may be considered to be relatively simple three-level systems.

For simplicity, consider a representative three-level atom whose ground state is labeled 1, and whose two upper (excited) states are 2 and 3 (Figure 20.8). The relative population of the two excited states is straightforward to obtain, but can involve a large number of coupled equations. Fortunately, transitions between all levels in Figure 20.3 are not equally likely. Because of the relatively weak radiation intensity in nebulae, induced transition rates in the coolant ions can usually be neglected. In fact, we may assume that only collisional excitation and de-excitation and spontaneous decay occur between the ground state and either excited state. Furthermore, we neglect transitions between levels 2 and 3 (this will be justified in examples below). Figure 20.8a shows these transitions. Dashed lines indicate collisional processes, and wavy lines indicate radiative processes. Under these assumptions, the number of ions per unit volume in each state is given by

$$n_3(C_{31} + A_{31}) = n_1 C_{13} = n_1 \frac{g_3}{g_1} C_{31} e^{-E_{13}/kT_e}, \quad (20.47)$$

$$n_2(C_{21} + A_{21}) = n_1 C_{12} = n_1 \frac{g_2}{g_1} C_{21} e^{-E_{12}/kT_e}, \quad (20.48)$$

where $E_{ij} = E_i - E_j$. The line emissivity from the transition $i \rightarrow j$ is just the product of the number density n_i of ions in the i^{th} excited state, the energy difference $E_{ij} = h\nu_{ij}$, and the spontaneous emission rate A_{ij}. Therefore the ratio of intensity emitted by the $3 \rightarrow 1$ transition to that emitted by the $2 \rightarrow 1$ transition is

$$\frac{j(3 \rightarrow 1)}{j(2 \rightarrow 1)} = \frac{n_3 h\nu_{31} A_{31}}{n_2 h\nu_{21} A_{21}} = \frac{g_3 A_{31} \nu_{31}}{g_2 A_{21} \nu_{21}} \left(\frac{1 + A_{21}/C_{21}}{1 + A_{31}/C_{31}} \right) e^{-E_{23}/kT_e}, \quad (20.49)$$

using (20.47) and (20.48) to eliminate n_3 and n_2. Before proceeding to specific processes, we should note two important general features of the relative line strength (20.49). First, if the two excited states are such that E_{23} is comparable to E_{12}, then the relative

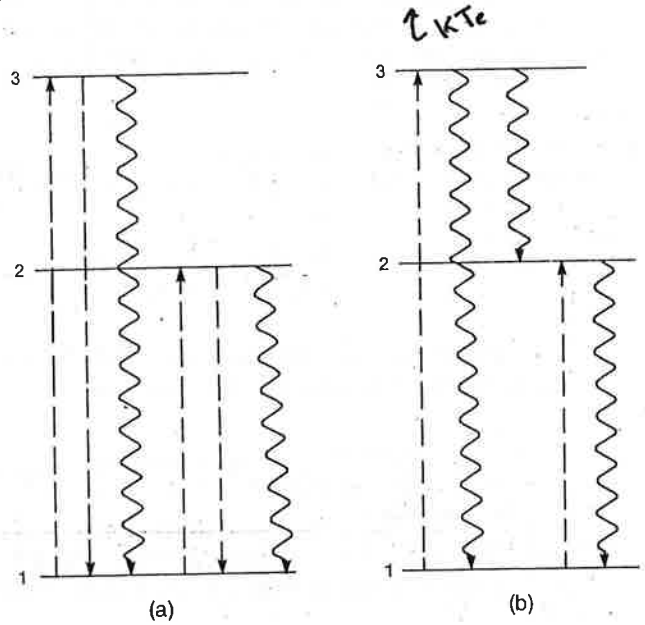

Figure 20.8. Three-level atom showing principal radiative transitions (wavy lines) and collisionally induced transitions (dashed lines): (a) transitions giving rise to (20.47) and (20.48); (b) transitions used to obtain (20.50) and (20.51).

strength will be very sensitive to T_e. If, on the other hand, $E_{23} \ll kT_e$, then the relative strength will vary most strongly with electron density (recall $C_{ij} \approx n_e/T_e^{1/2}$). Consequently, measurements of (20.49) for certain ions can be used to fix T_e, n_e, and the coolant abundances.

Most of the emission lines in HII regions and planetary nebulae that are generated by these collisional excitation–radiative de-excitation processes are optically forbidden. They occur with low transition probabilities (A $\sim$ 1 sec^{-1}). Gaseous nebulae are the most common instances of these lines in astronomy. Other instances are: (1) the solar corona; (2) the spectrum of the night sky; and (3) the aurora borealis.

Electron temperature measurements utilize the transitions $^1S_0 \rightarrow {}^1D_2$ ($\lambda = 4363$ Å), $^1D_2 \rightarrow {}^3P_2$ ($\lambda = 5007$ Å), and $^1D_2 \rightarrow {}^3P_1$ ($\lambda = 4959$ Å), which occur in [OIII] (Figure 20.3). All of these lie in the visible spectrum, the first with an energy of 2.84 eV, the other two with energies of nearly 2.51 eV, and all may be observed in most nebulae. Both excited states will be populated, and the relative populations will be a good indicator of T_e. We may consider as a reasonable approximation to [OIII] in nebulae a three-level system (as described in the preceding) in which excitation of the ^1S or ^1D levels is due to collisions, but the decay is radiative (no collisional de-excitation), an assumption that is reasonable as long as n_e is not too great. Furthermore, we shall allow the radiation decay $^1S \rightarrow {}^1D$. The possible transitions are shown in Figure 20.8. Setting up level densities as in (20.47) and (20.48), we can find immediately that the ratio of line intensity at $\lambda = 4363$ Å to that at $\lambda = 4959$ Å and $\lambda = 5007$ Å combined is

$$\frac{j(4363)}{j(5007) + j(4959)} \simeq \frac{n_3 h\nu_{32} A_{32}}{n_2 h\nu_{21} A_{21}} = \frac{g_3 \nu_{32} C_{31}}{g_2 \nu_{21} C_{21}} \frac{A_{32}}{A_{32} + A_{31}} e^{-E_{32}/kT_e}. \quad (20.50)$$

For [OIII], the energy difference $E_{32} = 2.84$ eV and the coefficient of the exponential is 0.12. Thus

$$\frac{j(4363)}{j(5007) + j(4959)} = 0.12\, e^{-32{,}900/T_e}, \quad (20.51)$$

where T_e is in K. This simple relation fits quite well for $n_e \lesssim 10^5$ cm^{-3}. A similar result can be found for [NII] ($E_{32} = 2.16$ eV, and the coefficient is 0.13). It is evident that small changes in T_e produce large shifts in the relative line strength. In fact, the ratio varies by nearly a factor of 10^2 when T_e varies from 6000 K to 2×10^4 K. Observations of the [OIII] ratio in HII regions give T_e in the range 8 to 9×10^3 K; for planetary nebulae, T_e is found to vary from 10 to 18×10^3 K. Measurements of the relative strength for the analogous transitions in [NII] yield $7{,}000 \lesssim T_e \lesssim 1.1 \times 10^4$ K in HII regions, and $10^4 \lesssim T_e \lesssim 1.5 \times 10^4$ K in planetary nebulae. Presumably the difference between [NII] and [OIII] measurements reflects the fact that the emission arises from different portions of the nebulae (see Figure 20.6).

The $^2D_{3/2} \rightarrow {}^4S_{3/2}$ ($\lambda = 3726$) and $^2D_{5/2} \rightarrow {}^4S_{3/2}$ ($\lambda = 3729$) transitions in [OII] are used to measure n_e in nebulae. If only collisional processes and radiative decay between the ^2D and ^4S states are considered, then we again have a simple three-level model as in Figure 20.8(a), except that $E_{23} \ll kT_e$, or $\nu_{21} \simeq \nu_{31}$. Proceeding as above, we easily find the relative line strength of the $\lambda = 3729$ Å and $\lambda = 3726$ Å transitions to be

$$\frac{j(3729)}{j(3726)} = \frac{g_3 A_{31}}{g_2 A_{21}} \left(\frac{1 + A_{21}/C_{21}}{1 + A_{31}/C_{31}} \right), \quad (20.52)$$

which depends weakly on T_e through C_{ij}. In fact, since $C_{ij} \approx n_e/T_e^{1/2}$, the ratio is sensitive to n_e. In relatively dilute regions $C_{ij} \rightarrow 0$, and the ratio reduces to

$$g_3 C_{31}/g_2 C_{21} = \Omega(3, 1)/\Omega(2, 1),$$

which for [OII] is 1.5. In the high-density limit, the ratio (20.52) approaches $g_3 A_{31}/g_2 A_{21} = 0.32$ for [OII]. At temperatures of order 10^3 to 10^4 K, the change in relative line strength is most sensitive to n_e. A similar set of transitions in the red occurs in [SII], and these are also used to measure n_e.

Electron number densities obtained in this way for HII regions vary from 10^2 to several times 10^3 cm^{-3} within individual nebulae. The denser regions are believed to be condensations. A gradual reduction in n_e from the center outward is also observed.

Line intensities from coolant ions in planetary nebulae are of limited use in measuring n_e, since at temperatures of 10^4 K or more, few ions are found in their lower excited states. The emission that is observed is believed to arise from condensations, or

from the outer regions of the nebula. Observed ratios for [OII] (20.39) imply that $n_e/T_e^{1/2}$ varies from roughly unity to about 400, with typical values around 40.

Problem 20.10. Derive the relative line strength (20.52) for the processes shown in Figure 20.8(a), and plot it as a function of $n_e/T_e^{1/2}$. For the [OII] transition rates, take $A_{31} = 4.2 \times 10^{-5}$ sec^{-1}, $A_{21} = 1.8 \times 10^{-4}$ sec^{-1}, $\Omega(3,1) = 0.88$ and $\Omega(2,1) = 0.59$.

The relative abundance of some intermediate-mass elements can also be found from line-strength measurements. For example, the $\lambda = 4959$ Å and $\lambda = 5007$ Å transitions in [OIII] are the dominant cooling mechanisms in some nebulae. To the extent that other cooling processes are small, the energy-balance equation (20.46) becomes

$$h\bar{\nu} = \frac{n(O^{+2})}{n(H^+)} e^{-\chi/kT_e}. \tag{20.53}$$

Examination of Figure 20.6 indicates that when [OIII] is likely to dominate the cooling rates, $n(O^{+2}) \approx n(O)$, the total abundance of oxygen, and similarly, $n(H^+) \approx n(H)$. Therefore, if T_e is known,

$$n(O)/n(H) \approx h\bar{\nu}\, e^{\chi/kT_e}. \tag{20.54}$$

Furthermore, if the strength of emission from other ions can be measured relative to the [OIII] lines, then some estimate of their abundances may be made as well.

20.7. Thermal Radio Emission

Diffuse nebulae and some types of galaxies are known to be radio sources. The simplest sources (in terms of their radio emission) have thermal spectra. One source of radio emission is a hot, tenuous plasma, such as is found in HII regions or in planetary nebulae (supernova remnants will be discussed in Chapter 25). The analysis of emission lines implies temperatures of order 10^4 K; so for wavelengths in the radio, $B_\nu(T) \approx 2kT/\lambda^2$. The observed intensity will be given by the solution to the transfer equation (5.38). Assuming that the plasma is in thermal equilibrium and that the temperature is uniform, I_ν will be given by (18.82), with T_s replaced by T. The primary contribution to the opacity of the gas κ_ν is from absorption caused by electron free-free transitions, or *Bremsstrahlung*, which was discussed in Section 6.4; so we obtain the opacity by the following argument.

In thermal equilibrium $j_\nu = I_\nu k_\nu = B_\nu(T)k_\nu$, and k_ν is given by (6.82) and (6.83) integrated over the electron velocity distribution. Denoting the emission rate per gram in the frequency interval ν to $\nu + d\nu$ by $j_\nu\, d\nu$, we find that, to within constant factors,

$$j_\nu\, d\nu \approx \frac{n_e n_i}{T^{1/2}} \mathrm{d}\nu. \tag{20.55}$$

The absorption rate is given by

$$k_\nu B_\nu(T) d\nu \approx \rho \kappa_\nu T \nu^2\, d\nu. \tag{20.56}$$

In equilibrium, these two rates must be equal, which gives the desired result

$$\rho\kappa_\nu \approx \frac{n_e^2}{T^{3/2}\nu^2}, \tag{20.57}$$

where we set $n_e = n_i$. The preceding arguments are not exact, and the actual opacity contains an additional weak dependence on T and ν of the form $\log(T^{3/2}/\nu)$, which is ignored in the following discussion.

According to (20.57), the plasma will be transparent at high frequencies, but becomes opaque at lower frequencies (longer wavelengths). Therefore, at long wavelengths, $\tau_\nu \ll 1$, and the intensity becomes

$$I_\nu \simeq \frac{2kT\nu^2}{c^2} \tau_\nu. \tag{20.58}$$

If the temperature is uniform throughout the emission region, then the optical depth becomes

$$\tau_\nu = \int_0^l \kappa_\nu \rho\, dr \approx \frac{\int_0^l n_e^2\, dr}{T^{3/2}\nu^2}. \tag{20.59}$$

The quantity $\int n_e^2\, dr$ is called the *emission measure*, and l is the length along the line of sight of the emitting region. Combining (20.58) and (20.59) yields

$$I_\nu \approx \frac{\int_0^l n_e^2\, dr}{T^{1/2}} \quad \text{for} \quad \tau_\nu \ll 1, \tag{20.60}$$